International Journal of Minerals, Metallurgy and Materials
Volume 28, Number 3, March 2021, Page 503
https://doi.org/10.1007/s12613-020-2193-y

Construction of TiO_2-pillared multilayer graphene nanocomposites as efficient photocatalysts for ciprofloxacin degradation

Xiong-feng Zeng, Jian-sheng Wang, Ying-na Zhao, Wen-li Zhang, and Meng-huan Wang

Hebei Provincial Laboratory of Inorganic Nonmetallic Materials, College of Materials Science and Engineering, North China University of Science and Technology, Tangshan 063210, China
(Received: 23 July 2020; revised: 9 September 2020; accepted: 11 September 2020)

Abstract: We successfully constructed TiO_2-pillared multilayer graphene nanocomposites (T-MLGs) via a facile method as follows: dodecanediamine pre-pillaring, ion exchange (Ti^{4+} pillaring), and interlayer *in-situ* formation of TiO_2 by hydrothermal method. TiO_2 nanoparticles were distributed uniformly on the graphene interlayer. The special structure combined the advantages of graphene and TiO_2 nanoparticles. As a result, T-MLGs with 64.3wt% TiO_2 showed the optimum photodegradation rate and adsorption capabilities toward ciprofloxacin. The photodegradation rate of T-MLGs with 64.3wt% TiO_2 was 78% under light-emitting diode light irradiation for 150 min. Meanwhile, the pseudo-first-order rate constant of T-MLGs with 64.3wt% TiO_2 was 3.89 times than that of pristine TiO_2. The composites also exhibited high stability and reusability after five consecutive photocatalytic tests. This work provides a facile method to synthesize semiconductor-pillared graphene nanocomposites by replacing TiO_2 nanoparticles with other nanoparticles and a feasible means for sustainable utilization of photocatalysts in wastewater control.

Keywords: pillared structure; titanium dioxide-pillared multilayer graphene nanocomposites; photocatalysis; ciprofloxacin

1. Introduction

Ciprofloxacin (CIP), a synthetic third-generation fluoroquinolone antibiotic, has widely been used for the efficient treatment of a number of bacterial infections [1]. However, the bio- and photo-degradation of CIP are difficult [2]. Hence, the investigation of the photocatalytic degradation of CIP by solar energy as a potential way to solve water pollution has attracted extensive research attention [3–8].

TiO_2 is the most widely studied and used as a photocatalyst in commercial applications because of its advantages [9–10]. However, the wide band gap and high photoelectron–hole recombination probability hinder the improvement of the photocatalytic performance of TiO_2 [11]. Strategies, including doping, nanostructuring, surface modification, and heterojunction construction, have been proposed to enhance the semiconductor properties of TiO_2 [7,12–16]. Graphene possesses a large specific surface area, excellent conduction, and chemical stability [17], resulting in good electron transfer and electron holding capacity. When TiO_2 combines with graphene, the photocatalytic activity of graphene–TiO_2 compositions is higher compared with pure TiO_2 [18–21] because of the effective charge transfer. Graphene–TiO_2 nanocomposites can be used not only in photocatalysis but also in dye-sensitized solar cells, ultraviolet photodetectors, and supercapacitors [22–26]. In addition, the good performances of these nanocomposites require a high interfacial contact [27–30] between graphene and TiO_2, which is the key to improve electron transfer and reducing electron–hole recombination, especially for photocatalysts [31]. TiO_2 nanoparticles anchoring onto graphene sheets by chemical interaction has been verified by a significantly enhanced photocatalytic activity [32].

To date, TiO_2 is usually loaded on the surface of multilayer or single-layer graphene in TiO_2–graphene nanocomposites [23–24,26,33–37]. Graphene–TiO_2 nanocomposite photocatalytic degradation rates differ, as will be compared later. To the best of our knowledge, TiO_2-pillared multilayer graphene nanocomposites (T-MLGs), which are formed through the insertion of TiO_2 nanoparticles into the interlayer spacing of multilayer graphene, have rarely been reported. Their special structure (pillared structure) can improve the photocatalytic efficiency by reducing photoelectron–hole recombination probability, which was verified by intercalating TiO_2 into the interlayer regions of layered materials, e.g., $HTaWO_6$ and $K_2Ti_4O_9$ [16,38]. Therefore, to enhance the

Corresponding author: Jian-sheng Wang E-mail: wangjiansheng@ncst.edu.cn

photocatalytic activity of TiO_2, we synthesized T-MLGs via a facile method as follows: dodecanediamine pre-pillaring, ion exchange (Ti^{4+} pillaring), and interlayer *in-situ* formation of TiO_2 by hydrothermal method. The preparation and photocatalytic activity for CIP degradation of T-MLGs were investigated in detail in this work.

2. Experimental

2.1. Synthesis of photocatalyst

All chemicals were of analytical reagent grade and used as received without any further purification.

2.1.1. Dodecanediamine pre-pillared graphene oxide intermediate

Dodecanediamine pre-pillared graphene oxide (GO) was prepared by Margarita's method [39]. First, 100 mg GO was dispersed in 16.5 mL deionized water via ultrasonication. Then, 4.16 mmol 1,12-dodecanediamine was dissolved in 17.5 mL ethanol, and the mixture was added dropwise to GO suspension under continuous stirring at room temperature for at least 48 h. Then, GO/dodecanediamine was centrifuged, washed with deionized water and absolute ethanol for several times, and dried at 80°C for 24 h. Finally, dodecanediamine pre-pillared GO was prepared successfully. GO with thickness of 0.8–1.2 nm was purchased from Nanjing XianFeng Nanomaterials Technology Co. Ltd., China.

2.1.2. Ion exchange (Ti^{4+} pillaring)

The TiO_2 sol was prepared before the Ti^{4+} exchange with dodecanediamine, which was prepared in accordance with the previously procedure reported by Chen *et al.* [40]. TiO_2 sol was adjusted to pH of 4–5 by 0.1 M ammonia solution. Then, the dodecanediamine pre-pillared GO was scattered dropwise into mixture mentioned above under magnetic stirring for 24 h to complete the Ti^{4+} exchange with dodecanediamine. After filtering, washing, and drying at 65°C for 24 h, the precursor powder was obtained.

2.1.3. Interlayer *in-situ* formation of TiO_2 by hydrothermal method

First, the precursor powder was dispersed in 30 mL deionized water via ultrasonication. Then, the mixed solution was transferred to a 50 mL Teflon-lined autoclave and reacted at 200°C for 4 h and cooled to 25°C naturally. Afterward, the precipitates were centrifuged, washed with deionized water and absolute ethanol until the filtrate was neutral, and dried at 80°C for 4 h. Finally, the T-MLGs were prepared successfully.

By controlling the amount of TiO_2 sol, T-MLGs with different TiO_2 weight percentages of 10.4wt%, 64.3wt%, and 94.1wt% were obtained and denoted as T-MLG-10.4, T-MLG-64.3, and T-MLG-94.1, respectively. TiO_2 as a control was prepared in the same experiment condition by hydrothermal method.

Fig. 1 illustrates the preparation process of T-MLGs.

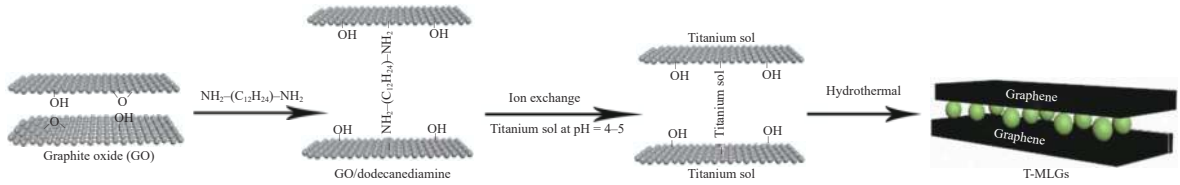

Fig. 1. Schematic diagram for synthesis process of T-MLGs.

2.2. Characterization

The crystal structures were analyzed by X-ray diffraction (XRD, D/MAX2500PC Rigaku, Cu K_α). The surface morphologies were investigated by scanning electron microscopy (SEM, Hitachi S-4800) and high-resolution transmission electron microscopy (HRTEM, JEM-2010). Raman spectrum was detected by DXR laser Raman spectroscopy. Fourier transform infrared spectra (FTIR) were measured on a Nicolet 470 FT-IR spectrometer. The photoluminescence (PL) spectra were obtained using a fluorescence spectrometer (PE, LS-S5). The excitation wavelength was 380 nm.

2.3. Photocatalytic degradation of the CIP solution

A total of 20 mg TiO_2 or 20 mg T-MLGs were dispersed in 40 mL CIP aqueous solution (15 mg/L). First, the mixtures were magnetically stirred for 30 min in the dark to establish the adsorption–desorption equilibrium of CIP on the sample surface. A 5 W light-emitting diode (LED) lamp (white light, wavelength $\lambda > 420$ nm) was employed as the light source. The CIP solution (3 mL) was extracted and centrifuged at a rate of 8000 r/min for 2 min every 30 min. The concentration change of CIP was determined using the spectrophotometric method (CE3021, Shanghai Precision & Scientific Instrument Co. Ltd., China) at 276 nm.

$$\text{Degradation rate} = \frac{C_0 - C_t}{C_0} \times 100\% \quad (1)$$

where C_0 and C_t are the concentrations of the initial CIP and CIP after t min irradiation, respectively.

3. Results and discussion

Fig. 2 shows the XRD patterns of GO, GO/dodecanediamine, GO/TiO_2 precursor, and T-MLGs with different TiO_2 contents. Compared with GO, the (001) peaks of

GO/dodecanediamine and GO/TiO_2 precursor shifted toward lower angles (from 11.1° to 7.3° and 11.1° to 7.67°, respectively), indicating the enlargement of interplanar distance as shown in Fig. 2(a). The large interplanar distance indicated that dodecanediamine or TiO_2 sol had intercalated into the lamellar GO sheets [41]. Fig. 2(b) shows the XRD patterns of T-MLG-10.4, T-MLG-64.3, T-MLG-94.1, and pure TiO_2. All samples showed a similar crystal structure, suggesting the formation of T-MLG nanocomposites after 200°C hydrothermal treatment. The intensity of the diffraction peaks increased as the TiO_2 content increased. The diffraction patterns had five broad peaks at 25.3°, 37.8°, 48.0°, 54.0°, and 62.7°, corresponding to the (101), (004), (200), (211), and (204) planes of TiO_2 (JCPDS No. 21-1272), respectively. However, no typical peak of graphene was observed in T-MLGs by XRD. Raman scattering was performed to confirm the existence of graphene in the nanocomposites.

As shown in Fig. 3(a), the Raman characteristic peaks at 160, 409, 531, and 654 cm^{-1}, which belong to TiO_2, were observed in all T-MLGs, thus confirming the existence of TiO_2 and consistent with the observation from the XRD in Fig. 2(b) [20]. Furthermore, two main peaks were observed at 1363 (peak D) and 1612 (peak G) cm^{-1} for all T-MLG samples, signifying the existence of graphene in T-MLGs. The intensity of graphene significantly decreased as the TiO_2 content increased (Fig. 3(a)). The reason may be the replacement of the graphene surface by TiO_2 nanoparticles [42].

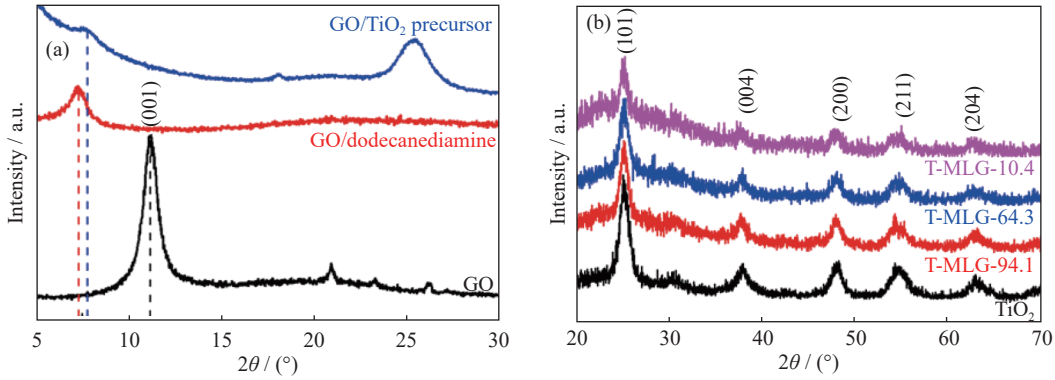

Fig. 2. XRD patterns of (a) GO, GO/dodecanediamine, and GO/TiO_2 precusor and (b) T-MLGs with different TiO_2 contents.

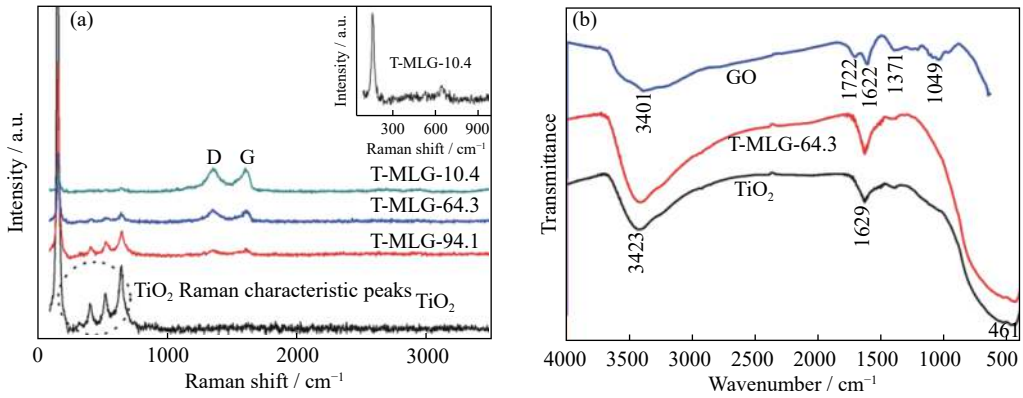

Fig. 3. Raman spectra of (a) pure TiO_2 and T-MLGs; (b) FTIR spectra of GO, T-MLG-64.3 and pure TiO_2. Inset in (a) shows partial enlarged drawing of T-MLG-10.4.

Although the existence of graphene and TiO_2 has been confirmed by Raman spectra, the connection between TiO_2 and graphene should be studied further by FTIR spectra. Fig. 3(b) displays the FTIR spectra of GO, T-MLG-64.3, and TiO_2. The absorption bands at 3401, 1622, and 1371 cm^{-1} in GO and T-MLG-64.3 indicated the presence of O–H stretching vibrations, skeletal ring vibrations of C=C, and tertiary C–OH groups [43], respectively. The absorption bands at 1722 and 1049 cm^{-1} showed the C=O and C–O stretching vibrations of COOH groups, respectively. However, both adsorption bands disappeared on T-MLG-64.3, indicating the reduction of GO after hydrothermal treatment [44–46]. Meanwhile, the peaks at 3423, 1629, and 461 cm^{-1} in TiO_2 nanoparticles and T-MLGs corresponded to the stretching and bending vibrations of –OH and Ti–O stretching mode, respectively. TiO_2 nanoparticles evidently existed in the T-MLGs. The broad absorption at 461 cm^{-1} in T-MLG-64.3 was considerably plumper than that in TiO_2, and this result was ascribed to the formation of Ti–O–C vibration in T-MLG-64.3 [44]. The presence of Ti–O–C bonds indicated the

chemical interaction between TiO_2 and graphene [47].

Figs. 4(a)–4(c) show the SEM micrographs of T-MLG-10.4, T-MLG-64.3, and T-MLG-94.1, respectively. T-MLGs with low TiO_2 content exhibited a plate-like morphology (Fig. 4(a)). With the increase in TiO_2 content, TiO_2 uniformly decorated and existed on the interlayer of graphene with high density (Figs. 4(b) and 4(c)). Moreover, the alveolate morphology of T-MLGs may be mainly attributed to the dehydroxylation and dehydration of TiO_2 gel precursor to oxide pillars after hydrothermal treatment [48]. The morphology of T-MLG-64.3 was further investigated by transmission electron microscopy (TEM). As shown in Figs. 4(d) and 4(e), TiO_2 nanoparticles were embedded in the graphene sheets. The HRTEM image of T-MLGs in Fig. 4(f) demonstrated that the TiO_2-pillared structure was obtained successfully. The evidence was the enlarged interplanar distance of graphene sheets from 0.34 to 0.516 nm (inset in Fig. 4(f)).

T-MLGs were prepared successfully via a facile method as follows: dodecanediamine pre-pillaring, ion exchange (Ti^{4+} pillaring), and interlayer *in-situ* formation of TiO_2 by hydrothermal method based on the above analysis.

The photocatalytic degradation of CIP (natural pH of 5.8) with 0.5 g/L photocatalysts was carried out in accordance with the preliminary experiment [49]. The adsorption property is an important factor affecting the photocatalytic performance. As shown in Fig. 5(a), the adsorption capacity of photocatalysts toward CIP after dark stirring for 30 min followed the order: T-MLG-64.3 > T-MLG-10.4 > T-MLG-94.1 > TiO_2. T-MLG-64.3 exhibited the best adsorption property. A blank without photocatalyst was also prepared under the same conditions to eliminate the effect of photolysis. Self-degradation rate was 3% after 150 min due to negli-

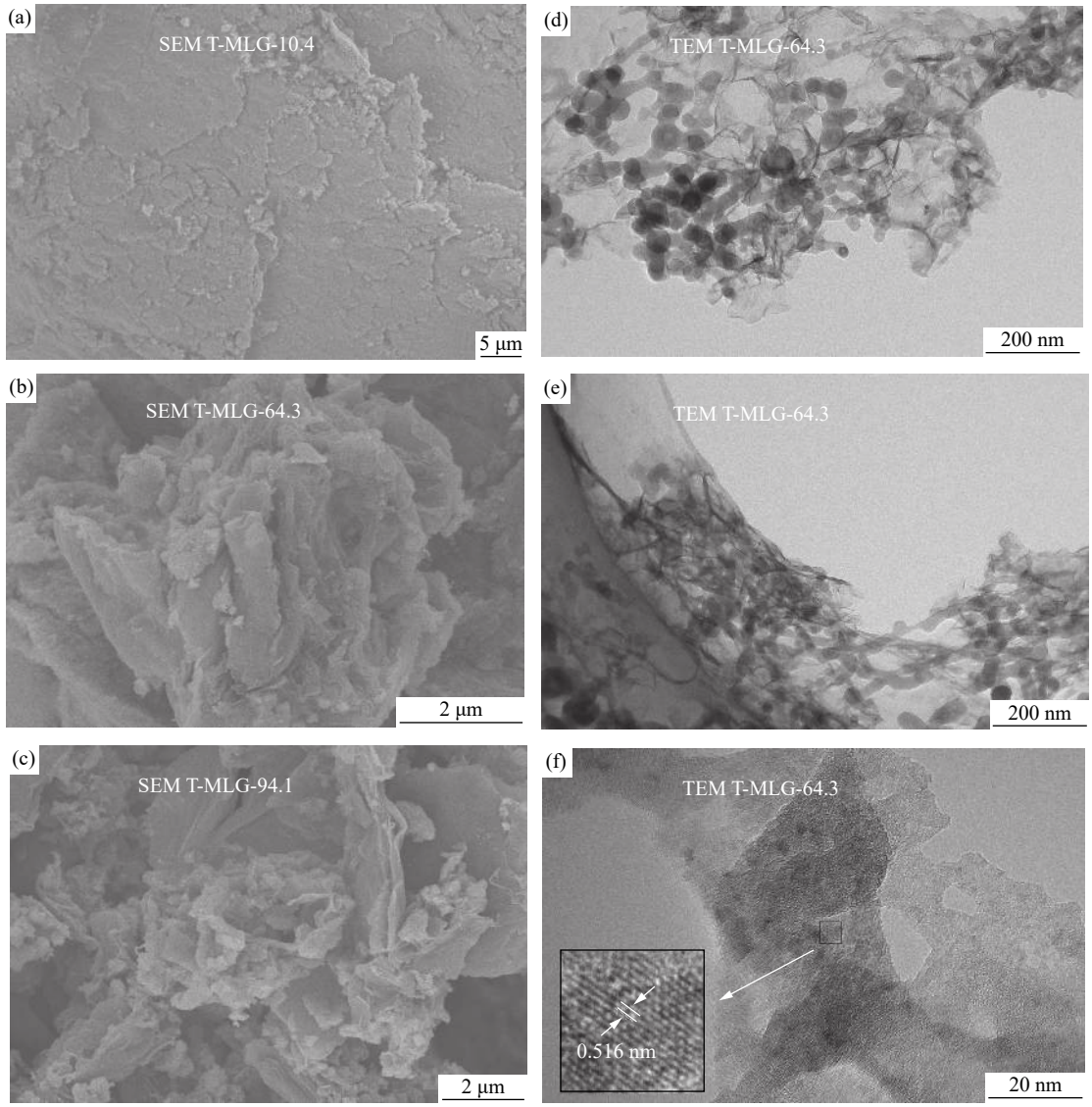

Fig. 4. SEM micrographs of (a) T-MLG-10.4, (b) T-MLG-64.3, and (c) T-MLG-94.1; (d)–(f) TEM images of T-MLG-64.3. Inset in (f) shows partial enlarged drawing.

gible photooxygenation reactions in the presence of molecular oxygen (Fig. 5(b)) [50]. To verify the enhanced photocatalytic performance of T-MLG-64.3, we performed comparative experiment for the degradation of CIP by using pure TiO_2 under the same conditions. The degradation efficiency of T-MLG-64.3 reached 78%, which was notably better than that of pure TiO_2 (42%) (Fig. 5(b)). Fig. 5(c) shows the photocatalytic degradation of CIP kinetics and the fitting results, which followed pseudo-first-order kinetics. The apparent reaction rate constant of T-MLG-64.3 was as much as 3.89 times than that of pure TiO_2. Five cycles of the photocatalytic experiments were conducted to examine the photostability and structure stability of T-MLGs, and one cycle lasted for 150 min. Fig. 5(d) offered the evidence that pillared structure nanocomposites are reusable and stable in recycling photocatalytic degradation experiments. After each cycle, the photocatalyst was washed and centrifuged for several times and finally irradiated under simulated sunlight for 60 min to ensure that the CIP molecules were removed completely. For comparison, the degradation rates of different organic pollutants over different kinds of graphene/TiO_2 composites and TiO_2 are listed in Table 1.

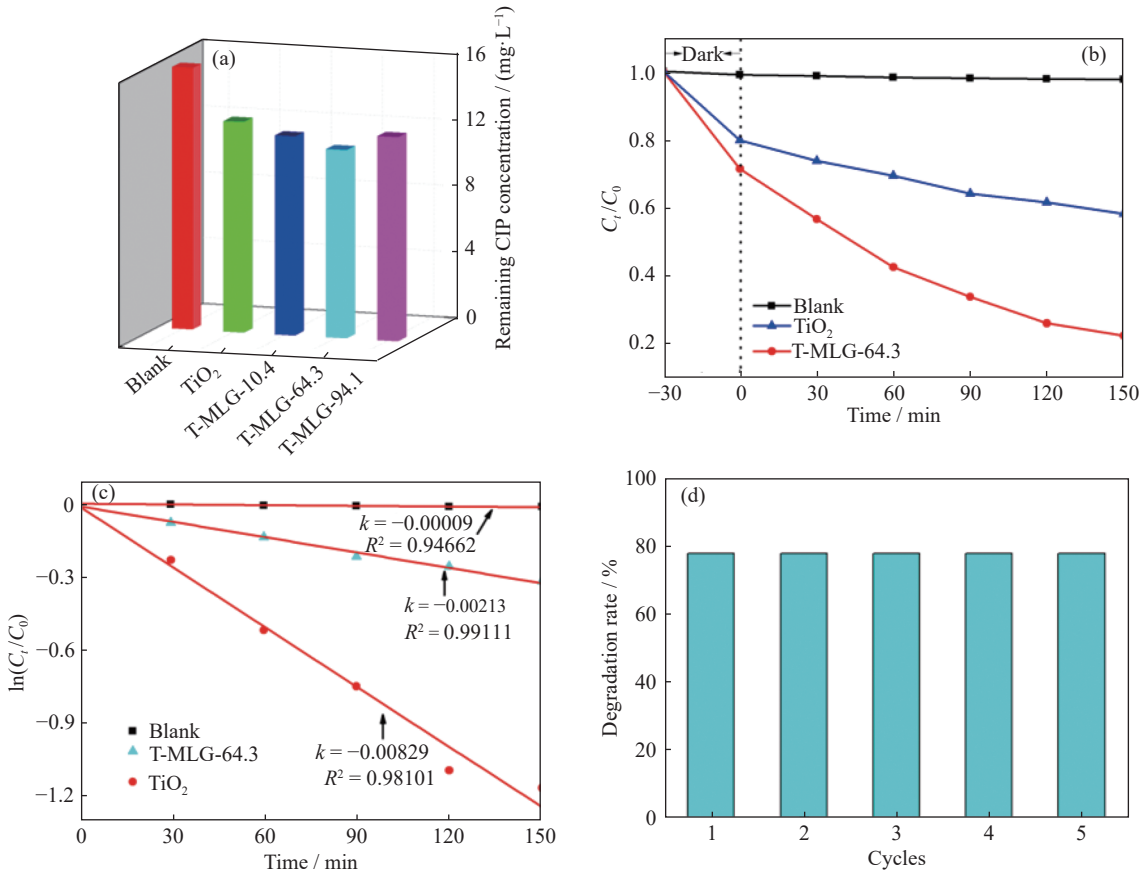

Fig. 5. (a) Adsorption of CIP in presence of different photocatalysts; (b) photocatalytic degradation of CIP; (c) pseudo-first order kinetics curves of the photocatalytic degradation of CIP (*k*—Apparent reaction rate constant; R^2—Coefficient of determination); (d) photo-degradation rates of CIP after repeated cycles (irradiation time of 150 min).

Table 1. Photocatalytic properties of graphene/TiO_2 composites in comparison with pure TiO_2

Organic pollutant	Irradiation system	Graphene content in graphene/TiO_2 composite	Degradation rate of pollutant / %		Ref.
			Graphene/TiO_2 composite	Pure TiO_2	
Methylene blue	Sunlight	8wt%	98.67 (45 min)	52 (2 h)	[51]
Ciprofloxacin	Sunlight	8wt%	96.73 (60 min)	65.52 (60 min)	[51]
Rhodamine-B	Solar light	0.09 g	98 (60 min)	42 (60 min)	[18]
Methylene blue	UV lamp (λ = 365 nm)	0.01 g	~97 (150 min)	~58 (150 min)	[32]
Methylene blue	LED lamp (λ > 420 nm)	0.01 g	~67 (150 min)	~58 (150 min)	[32]
Methylene blue	UV lamp	75wt%	~61 (70 min)	~35 (70 min)	[52]
Ciprofloxacin	LED lamp (λ > 420 nm)	35.7wt%	78 (150 min)	42 (150 min)	This work

The PL spectroscopy intensity of T-MLG-64.3 was lower than that of pure TiO_2 (Fig. 6). A high PL intensity indicates the easy recombination of electrons and holes [49,53]. Thus, when TiO_2 intercalated into the interlayer of graphene to form a TiO_2-pillared structure, graphene instantly accepted the photoinduced electron to reduce the recombination of electrons and holes and boost the electron–hole separation in TiO_2.

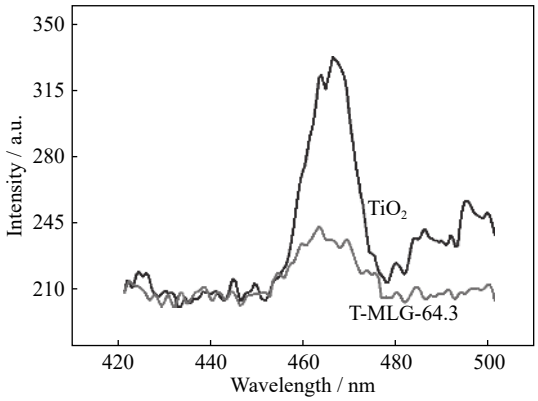

Fig. 6. PL spectra of pure TiO_2 and T-MLG-64.3 (excitation: 380 nm).

The active species capture experiment was conducted in this study to determine the active species that play the main role in the photocatalytic process of CIP degradation. 1 mmol·L^{-1} isopropyl alcohol (IPA), 1 mmo·L^{-1} triethanolamine (TEOA), and 0.1 mmol·L^{-1} benzoquinone (BQ) were added as scavengers for hydroxyl radical (·OH), hole (h^+), and superoxide radical ($\cdot O_2^-$) to CIP solution in the presence of T-MLG-64.3 photocatalyst, respectively. Other experimental conditions were the same as given for the photocatalytic degradation of CIP. Fig. 7 shows the different degradation rates after adding scavengers and the significant role of active species during photocatalysis. The degradation rates of CIP decreased from 78% of the blank to 63.8%, 16.9%, and 33.8% with IPA, TEOA, and BQ, respectively. Therefore, the hole provided the greatest contribution to CIP decomposition, followed by superoxide radical and then hydroxyl radical. The major photocatalytic process for CIP degradation using T-MLG-64.3 was proposed with the following reactions (2)–(9).

$$\text{T-MLGs} + h\nu \rightarrow h^+(TiO_2) + e^-(\text{graphene}) \quad (2)$$

$$e^- + O_2 \rightarrow \cdot O_2^- \quad (3)$$

$$\cdot O_2^- + H^+ \rightarrow \cdot OOH \quad (4)$$

$$2 \cdot OOH \rightarrow O_2 + H_2O_2 \quad (5)$$

$$H_2O_2 + e^- \rightarrow \cdot OH + OH^- \quad (6)$$

$$h^+ + OH^- \rightarrow \cdot OH \quad (7)$$

$$\cdot OH + CIP \rightarrow \text{Products} \quad (8)$$

$$h^+ + CIP \rightarrow \text{Products} \quad (9)$$

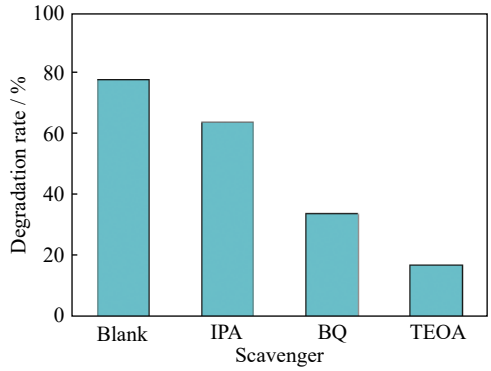

Fig. 7. Photocatalytic degradation rates of CIP for T-MLG-64.3 at presence of different scavengers after 150 min irradiation.

4. Conclusion

In summary, we constructed a new pillared structure of T-MLGs via a facile method as follows: dodecanediamine pre-pillaring, ion exchange (Ti^{4+} pillaring), and interlayer *in-situ* formation of TiO_2 by hydrothermal method. We proved through various testing means that TiO_2 nanoparticles had intercalated into the interlayer of graphene to form a TiO_2-pillared structure. T-MLG with 64.3wt% TiO_2 showed the optimum photodegradation rate and adsorption capabilities toward CIP. The photodegradation rate of T-MLG with 64.3wt% TiO_2 was 78% under LED light irradiation for 150 min. Meanwhile, the pseudo-first-order rate constant of T-MLG with 64.3wt% TiO_2 was 3.89 times that of pristine TiO_2. Such result was mainly attributed to the special structure with enhanced photoinduced electron–hole separation in TiO_2. Furthermore, the material exhibited high stability and reusability after five consecutive photocatalytic tests. The hole and superoxide radical were determined as the main contributors of CIP degradation. This work provides a facile method to synthesize semiconductor-pillared graphene nanocomposites by replacing TiO_2 nanoparticles with other nanoparticles and a feasible technical for the sustainable utilization of photocatalysts in wastewater control.

Acknowledgements

This work was financially supported by the Youth Fund of Hebei Province Education Department, China (No. QN2017117) and the Hebei Natural Science Funds for the Joint Research of Iron and Steel, China (Nos. E2019209374 and E2015209278).

References

[1] G.K. Dimitrakakis, E. Tylianakis, and G.E. Froudakis, Pillared graphene: A new 3-D network nanostructure for enhanced hy-

drogen storage, *Nano Lett.*, 8(2008), No. 10, p. 3166.
[2] A.B. Caracciolo, P. Grenni, J. Rauseo, N. Ademollo, M. Cardoni, L. Rolando, and L. Patrolecco, Degradation of a fluoroquinolone antibiotic in an urbanized stretch of the River Tiber, *Microchem. J.*, 136(2018), p. 43.
[3] M. Malakootian, A. Nasiri, and M.A. Gharaghani, Photocatalytic degradation of ciprofloxacin antibiotic by TiO_2 nanoparticles immobilized on a glass plate, *Chem. Eng. Commun.*, 207(2020), No. 1, p. 56.
[4] X. Hu, X.J. Hu, Q.Q. Peng, L. Zhou, X.F. Tan, L.H. Jiang, C.F. Tang, H. Wang, S.H. Liu, Y.Q. Wang, and Z.Q. Ning, Mechanisms underlying the photocatalytic degradation pathway of ciprofloxacin with heterogeneous TiO_2, *Chem. Eng. J.*, 380(2020), art. No. 122366.
[5] S.S. Imam, R. Adnan, and N.H.M. Kaus, Photocatalytic degradation of ciprofloxacin in aqueous media: A short review, *Toxicol. Environ. Chem.*, 100(2018), No. 5-7, p. 518.
[6] P.W. Huo, Y.F. Tang, M.J. Zhou, J.Z. Li, Z.F. Ye, C.C. Ma, L.B. Yu, and Y.S. Yan, Fabrication of $ZnWO_4$–CdS heterostructure photocatalysts for visible light induced degradation of ciprofloxacin antibiotics, *J. Ind. Eng. Chem.*, 37(2016), p. 340.
[7] X. Zheng, S.Y. Chen, Z. Chen, R.Y. Chen, and X. Chen, Preparation of carbon-coated TiO_2–CeO_2 fibers for the photocatalytic degradation of ciprofloxacin, *Chin. J. Appl. Chem.*, 30(2013), No. 11, p. 1326.
[8] M. El-Kemary, H. El-Shamy, and I. El-Mehasseb, Photocatalytic degradation of ciprofloxacin drug in water using ZnO nanoparticles, *J. Lumin.*, 130(2010), No. 12, p. 2327.
[9] R. Djellabi, M.F. Ghorab, G. Cerrato, S. Morandi, S. Gatto, V. Oldani, A.D. Michele, and C.L. Bianchi, Photoactive TiO_2–montmorillonite composite for degradation of organic dyes in water, *J. Photochem. Photobiol. A*, 295(2014), p. 57.
[10] K. Nakata and A. Fujishima, TiO_2 photocatalysis: Design and applications, *J. Photochem. Photobiol. C*, 13(2012), No. 3, p. 169.
[11] Y.X. Zhang, Z.Y. Zhou, T. Chen, H.T. Wang, and W.J. Lu, Graphene TiO_2 nanocomposites with high photocatalytic activity for the degradation of sodium pentachlorophenol, *J. Environ. Sci.*, 26(2014), No. 10, p. 2114.
[12] J.J. Cai, S. Li, and G.W. Qin, Interface engineering of Co_3O_4 loaded $CaFe_2O_4$/Fe_2O_3 heterojunction for photoelectrochemical water oxidation, *Appl. Surf. Sci.*, 466(2019), p. 92.
[13] J.J. Cai, H. Chen, S.L. Ding, and Q. Xie, Promoting photocarrier separation for photoelectrochemical water splitting in α-Fe_2O_3@C, *J. Nanopart. Res.*, 21(2019), art. No. 153.
[14] J.J. Cai, S.L. Ding, G. Chen, Y.L. Sun, and Q. Xie, *In situ* electrodeposition of mesoporous aligned α-Fe_2O_3 nanoflakes for highly sensitive nonenzymatic H_2O_2 sensor, *Appl. Surf. Sci.*, 456(2018), p. 302.
[15] J.J. Cai, H. Chen, C.X. Liu, S.Q. Yin, H.J. Li, L.C. Xu, H. Liu, and Q. Xie, Engineered Sn- and Mg-doped hematite photoanodes for efficient photoelectrochemical water oxidation, *Dalton Trans.*, 49(2020), No. 32, p. 11282.
[16] X.T. Pian, B.Z. Lin, Y.L. Chen, J.D. Kuang, K.Z. Zhang, and L.M. Fu, Pillared nanocomposite TiO_2/Bi-doped hexaniobate with visible-light photocatalytic activity, *J. Phys. Chem. C*, 115(2011), No. 14, p. 6531.
[17] B.C. Qiu, M.Y. Xing, and J.L. Zhang, Mesoporous TiO_2 nanocrystals grown *in situ* on graphene aerogels for high photocatalysis and lithium-ion batteries, *J. Am. Chem. Soc.*, 136(2014), No. 16, p. 5852.
[18] V.R. Posa, V. Annavaram, J.R. Koduru, P. Bobbala, Madhavi V, and A.R. Somala, Preparation of graphene–TiO_2 nanocomposite and photocatalytic degradation of Rhodamine-B under solar light irradiation, *J. Exp. Nanosci.*, 11(2016), No. 9, p. 722.
[19] S. Kanan, M.A. Moyet, R.B. Arthur, and H.H. Patterson, Recent advances on TiO_2-based photocatalysts toward the degradation of pesticides and major organic pollutants from water bodies, *Catal. Rev. Sci. Eng.*, 62(2020), No. 1, p. 1.
[20] P. Wang, J. Wang, X.F. Wang, H.G. Yu, J.G. Yu, M. Lei, and Y.G. Wang, One-step synthesis of easy-recycling TiO_2–rGO nanocomposite photocatalysts with enhanced photocatalytic activity, *Appl. Catal. B*, 132-133(2013), p. 452.
[21] G.X. Hu and B. Tang, Photocatalytic mechanism of graphene/titanate nanotubes photocatalyst under visible-light irradiation, *Mater. Chem. Phys.*, 138(2013), No. 2-3, p. 608.
[22] F.W. Low and C.W. Lai, Recent developments of graphene–TiO_2 composite nanomaterials as efficient photoelectrodes in dye-sensitized solar cells: A review, *Renewable Sustainable Energy Rev.*, 82(2018), p. 103.
[23] F.X. Liang, J.Z. Wang, Y. Wang, Y. Lin, L. Liang, Y. Gao, and L.B. Luo, Single-layer graphene/titanium oxide cubic nanorods array/FTO heterojunction for sensitive ultraviolet light detection, *Appl. Surf. Sci.*, 426(2017), p. 391.
[24] D.Y. Zhang, C.W. Ge, J.Z. Wang, T.F. Zhang, Y.C. Wu, and F.X. Liang, Single-layer graphene–TiO_2 nanotubes array heterojunction for ultraviolet photodetector application, *Appl. Surf. Sci.*, 387(2016), p. 1162.
[25] J. Chen, C. Li, and G.Q. Shi, Graphene materials for electrochemical capacitors, *J. Phys. Chem. Lett.*, 4(2013), No. 8, p. 1244.
[26] J.Q. Yang, Y.B. Hu, C.G. Jin, L.J. Zhuge, and X.M. Wu, Preparation of TiO_2/single layer graphene composite films via a novel interface-facilitated route, *Appl. Surf. Sci.*, 503(2020), art. No. 144334.
[27] C.J. Xu, Y.T. Wu, S. Li, J. Zhou, J. Chen, M. Jiang, H.D. Zhao, and G.W. Qin, Engineering the epitaxial interface of Pt–CeO_2 by surface redox reaction guided nucleation for low temperature CO oxidation, *J. Mater. Sci. Technol.*, 40(2020), p. 39.
[28] Y.L. Liu, H. Chen, C.J. Xu, Y.M. Sun, S. Li, M. Jiang, and G.W. Qin, Control of catalytic activity of nano‐Au through tailoring the fermi level of support, *Small*, 15(2019), No. 34, art. No. 1901789.
[29] F. Cao, X. Yang, C. Shen, X. Li, J.M. Wang, G.W. Qin, S. Li, X.Y. Pang, and G.Q. Li, Electrospinning synthesis of transition metal alloy nanoparticles encapsulated in nitrogen-doped carbon layers as an advanced bifunctional oxygen electrode, *J. Mater. Chem. A*, 8(2020), No. 15, p. 7245.
[30] X.Q. Cao, J. Zhou, H.N. Wang, S. Li, W. Wang, and G.W. Qin, Abnormal thermal stability of sub-10 nm Au nanoparticles and their high catalytic activity, *J. Mater. Chem. A*, 7(2019), No. 18, p. 10980.
[31] H.H. Liu, D.B. Zhu, H. Shi, and X. Shao, Fabrication of a contamination-free interface between graphene and TiO_2 single crystals, *ACS Omega*, 1(2016), No. 2, p. 168.
[32] Y.L. Min, K. Zhang, W. Zhao, F.C. Zheng, Y.C. Chen, and Y.G. Zhang, Enhanced chemical interaction between TiO_2 and graphene oxide for photocatalytic decolorization of methylene blue, *Chem. Eng. J.*, 193-194(2012), p. 203.
[33] Y.H. Zhang, Z.R. Tang, X.Z. Fu, and Y.J. Xu, TiO_2–graphene nanocomposites for gas-phase photocatalytic degradation of volatile aromatic pollutant: Is TiO_2–graphene truly different from other TiO_2–carbon composite materials?, *ACS Nano*, 4(2010), No. 12, p. 7303.
[34] Z.Y. Zhang, F. Xiao, Y.L. Guo, S. Wang, and Y.Q. Liu, One-pot self-sssembled three-dimensional TiO_2–graphene hydrogel

with improved adsorption capacities and photocatalytic and electrochemical activities, *ACS Appl. Mater. Interfaces*, 5(2013), No. 6, p. 2227.

[35] F.H. Zhao, B.H. Dong, R.J. Gao, G. Su, W. Liu, L. Shi, C.H. Xia, and L.X. Cao, A three-dimensional graphene–TiO_2 nanotube nanocomposite with exceptional photocatalytic activity for dye degradation, *Appl. Surf. Sci.*, 351(2015), p. 303.

[36] A.K. Singh, V. Chaudhary, A.K. Singh, and S.R.P. Sinha, Effect of TiO_2 nanoparticles on electrical properties of chemical vapor deposition grown single layer graphene, *Synth. Met.*, 256(2019), art. No. 116155.

[37] A.K. Singh, V. Chaudhary, A.K. Singh, and S.R.P. Sinha, Tailoring of electrical properties of TiO_2 decorated CVD grown single-layer graphene by HNO_3 molecular doping, *Synth. Met.*, 264(2020), art. No. 116389.

[38] M.A.M. Júnior, A. Morais, and A.F. Nogueira, Boosting the solar-light-driven methanol production through CO_2 photoreduction by loading Cu_2O on TiO_2-pillared $K_2Ti_4O_9$, *Microporous Mesoporous Mater.*, 234(2016), p. 1.

[39] M. Herrera-Alonso, A.A. Abdala, M.J. McAllister, I.A. Aksay, and R.K. Prud'homme, Intercalation and stitching of graphite oxide with diaminoalkanes, *Langmuir*, 23(2007), No. 21, p. 10644.

[40] R.Y. Chen, J.W. Wang, H.N. Wang, W. Yao, and J. Zhong, Photocatalytic degradation of methyl orange in aqueous solution over titania-pillared α-zirconium phosphate, *Solid State Sci.*, 13(2011), No. 3, p. 630.

[41] F.F. Guo, W. Xing, J. Zhou, L.M. Zhao, J.B. Zeng, Z. Liu, Q.Z. Xue, and Z.F. Yan, Studies in the capacitance properties of diaminoalkane-intercalated graphene, *Electrochim. Acta*, 148(2014), p. 220.

[42] S. Zargari, R. Rahimi, A. Ghaffarinejad, and A. Morsali, Enhanced visible light photocurrent response and photodegradation efficiency over TiO_2–graphene nanocomposite pillared with tin porphyrin, *J. Colloid Interface Sci.*, 466(2016), p. 310.

[43] C. Nethravathi and M. Rajamathi, Chemically modified graphene sheets produced by the solvothermal reduction of colloidal dispersions of graphite oxide, *Carbon*, 46(2008), No. 14, p. 1994.

[44] H. Zhang, X.J. Lv, Y.M. Li, Y. Wang, and J.H. Li, P25–graphene composite as a high performance photocatalyst, *ACS Nano*, 4(2010), No. 1, p. 380.

[45] W.W. Zhang, H.L. Guo, H.Q. Sun, and R.C. Zeng, Hydrothermal synthesis and photoelectrochemical performance enhancement of TiO_2/graphene composite in photo-generated cathodic protection, *Appl. Surf. Sci.*, 382(2016), p. 128.

[46] S.X. Min, F. Wang, and G.X. Lu, Graphene-induced spatial charge separation for selective water splitting over TiO_2 photocatalyst, *Catal. Commun.*, 80(2016), p. 28.

[47] T.-D. Nguyen-Phan, V.H. Pham, E.W. Shin, H.-D. Pham, S. Kim, J.S. Chung, E.J. Kim, and S.H. Hur, The role of graphene oxide content on the adsorption-enhanced photocatalysis of titanium dioxide/graphene oxide composites, *Chem. Eng. J.*, 170(2011), No. 1, p. 226.

[48] X.R. Fan, B.Z. Lin, H. Liu, L.W. He, Y.L. Chen, and B.F. Gao, Remarkable promotion of photocatalytic hydrogen evolution from water on TiO_2-pillared titanoniobate, *Int. J. Hydrogen Energy*, 38(2013), No. 2, p. 832.

[49] N. Li, J. Zhang, Y. Tian, J.H. Zhao, J. Zhang, and W. Zuo, Precisely controlled fabrication of magnetic 3D γ-Fe_2O_3@ZnO core-shell photocatalyst with enhanced activity: Ciprofloxacin degradation and mechanism insight, *Chem. Eng. J.*, 308(2017), p. 377.

[50] A. Salma, S. Thoröe-Boveleth, T.C. Schmidt, and J. Tuerk, Dependence of transformation product formation on pH during photolytic and photocatalytic degradation of ciprofloxacin, *J. Hazard. Mater.*, 313(2016), p. 49.

[51] S.A. Khan, Z. Arshad, S. Shahid, I. Arshad, K. Rizwan, M. Sher, and U. Fatima, Synthesis of TiO_2/graphene oxide nanocomposites for their enhanced photocatalytic activity against methylene blue dye and ciprofloxacin, *Composites Part B*, 175(2019), art. No. 107120.

[52] J.J. Guo, S.M. Zhu, Z.X. Chen, Y. Li, Z.Y. Yu, Q.L. Liu, J.B. Li, C.L. Feng, and D. Zhang, Sonochemical synthesis of TiO_2 nanoparticles on graphene for use as photocatalyst, *Ultrason. Sonochem.*, 18(2011), No. 5, p. 1082.

[53] H.W. Chen, Y. Ku, and Y.L. Kuo, Effect of Pt/TiO_2 characteristics on temporal behavior of *o*-cresol decomposition by visible light-induced photocatalysis, *Water Res.*, 41(2007), No. 10, p. 2069.